Current Applied Physics 16 (2016) 691–695

Contents lists available at ScienceDirect

Current Applied Physics

journal homepage: www.elsevier.com/locate/cap

Comparison of hydrogen sulfide gas and sulfur powder for synthesis of molybdenum disulfide nanosheets

Jusang Park [a], Jeong-Gyu Song [a], Taejin Choi [a], Sangwan Sim [a], Hyunyong Choi [a], Sang Wook Han [b], Han-Bo-Ram Lee [c], Soo-Hyun Kim [d], Hyungjun Kim [a, *]

[a] School of Electrical and Electronic Engineering, Yonsei University, Seoul 120-749, South Korea
[b] Department of Physics and Energy Harvest–Storage Research Center, University of Ulsan, Ulsan 680-749, South Korea
[c] Materials Science and Engineering, Incheon National University, Incheon 406-840, South Korea
[d] School of Materials Science and Engineering, Yeungnam University, Gyeongsan-si 712-749, South Korea

ARTICLE INFO

Article history:
Received 29 July 2015
Received in revised form
12 February 2016
Accepted 31 March 2016
Available online 1 April 2016

Keywords:
Hydrogen sulfide
Sulfur powder
Transition metal dichalcogenides (TMDC)
2D nanosheet
Selectable area growth

ABSTRACT

Layered transition metal dichalcogenides (TMDCs) have the potential to be used as an alternative to graphene in nano applications, because of their unique opto-electric properties. However, the large-scale synthesis of TMDCs has not been thoroughly investigated with different sulfurization agents, nor have the effects of defects and vacancies on such synthesis been determined. This study therefore looks at the synthesis of MoS_2 nanosheets from a thin Mo film to compare the effects of using H_2S gas or sulfur powder as the sulfurization agent. In either case, a four-layered nanosheet is obtained; however, the good stoichiometry of MoS_2, smallest defects, and fewest vacancies are obtained using H_2S.

1. Introduction

Layered transition metal dichalcogenides (TMDCs) have recently drawn significant attention for use as next generation nano-electronics [1], thin film transistors [2], logic circuits [3], sensors [4], catalysts [5,6], and optoelectronic devices [7,8]. The physical, electrical, and optical properties of TMDCs have so far mostly been studied through physical exfoliation of nanosheets and their transfer onto suitable substrates [9–11]. However, nanosheets with a large surface area can only be achieved through synthesis directly onto a substrate. Recently, the layered MoS_2 was most famous in TMDCs because the exotic properties of optical and electrical. The early stage method of synthesizing MoS_2 is the sulfurization of metal and metal-oxide films using a sulfurization agent [12–16], and good quality MoS_2 and WS_2 nanosheets have been achieved through chemical vapor deposition (CVD) [17–20].

There is a potential problem in the use of sulfur powder as a sulfurization agent, namely the fact that its vaporization requires temperatures above 200 °C, and that its vapor has a S_8 crown ring structure that leads to inhomogeneous sulfurization [21]. In contrast, H_2S gas has a simple molecular structure with a low decomposition energy, ensuring a reliable and homogeneous reaction [22,23]. The synthesis of MoS_2 nanostructures has been previously achieved using H_2S gas [24, 25], but was found to result in S vacancies forming near nanocluster edges, grain boundaries, and defect sites [26, 27, 28] that greatly affected the optical and electrical properties [27, 28]. However, as there has been no comparative study of different sulfurization agents, this study compares the synthesis of MoS_2 using H_2S gas with that using sulfur powder at temperatures of 1000 and 750 °C. The intrinsic properties of the MoS_2 nanosheets obtained are also investigated through pump probe measurements, though the ease with which MoS_2 readily changes its electrical properties prevented these from being included.

2. Experimental section

The single-crystal SiO_2 and MgO substrates were prepared by ultrasonic cleaning in acetone, IPA, and DI water for 10 min each. For metal sulfurization, 5 or 10 nm Mo metal films were deposited by sputtering for 5 or 10 s, respectively. Fig. 1 (a) shows the

* Corresponding author.
E-mail address: hyungjun@yonsei.ac.kr (H. Kim).

http://dx.doi.org/10.1016/j.cap.2016.03.022
1567-1739/

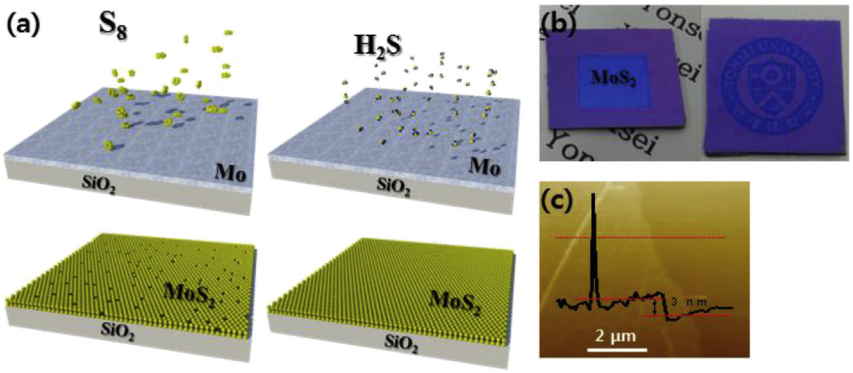

Fig. 1. (a) Schematic illustration of the sulfurization process. (b) Optical images of MoS_2 layers grown on a SiO_2 substrate. (c) AFM image of a four-layer MoS_2 nanosheet ~4 nm in thickness on a SiO_2/Si substrate.

differences in the sulfurization process depending on whether initial sulfurization in a tube type furnace at 500 °C was carried out using 5 sccm of H_2S gas or 3 g of sulfur powder (introduced at 120 °C) under a 50 sccm flow of Ar. Following this initial sulfurization, the temperature was increased to 750 or 1000 °C and held for 10 min to enhance the quality of the MoS_2 nanosheet. The sample preparation conditions are summarized in Fig. 2.

To measure the thickness of the MoS_2 nanosheets produced, each was measured by atomic force microscopy (AFM). Differences between the two different sulfurization methods were assessed by characterizing the different nanosheets using Raman spectroscopy, X-ray photoemission spectroscopy (XPS), tunneling electron microscopy (TEM), and pump probe measurement. The XPS measurements were performed at the 09A beam line of the National Synchrotron Radiation Research Center (NSRRC) in Hsinchu, Taiwan, with all data being obtained at a base pressure of less than 1×10^{-9} mbar.

The electrical characteristics and physical properties of the MoS_2 nanosheet were analyzed using ultrafast pump-probe methods so as to prevent any contamination or damage. These measurements were carried out with a visible probe range based on a 250 KHz Ti:sapphire laser system (Coherent RegA 9050) producing 50 fs pulses at 800 nm. A white-light continuum was created by focusing these 800 nm pulses into a sapphire disk, with 400 nm pulses being generated by a second harmonic.

3. Results and discussion

As shown in Fig. 1(b), large-area MoS_2 nanosheet with a uniform color was selectively grown using H_2S gas. After transferring it onto a clean SiO_2 substrate, an AFM line profile (Fig. 1(c)) was used to determine its thickness as 3 nm, which equates to four layers of MoS_2 nanosheet.

Fig. 2(a) shows the Raman spectra of MoS_2 nanosheets, prepared under various conditions (Fig. 2), from which the width of each peak can be used to determine the crystallinity of the sample [29, 30]. That is, the 24 cm^{-1} gap between the E^1_{2g} and A^1_g peaks corresponds to four layers of the MoS_2 nanosheet [30], and therefore confirms the AFM-measured thickness. Note also that the Si peak is normalized to allow such comparison between the intensities and widths of the E^1_{2g} and A_{1g} peaks. Fig. 2(b) shows the peak distance as a function of the Mo film thickness, suggesting a strong relation between the thickness of the MoS_2 nanosheets and the Mo films. There is, however, a poor conformity to the Raman spectrum when the number of layers exceeds four, with the larger intensity ratio of sample H10 indicating that a good crystallinity can be obtained by annealing at 1000 °C with H_2S gas. The full-width at half maximum (FWHM) values of the Raman peak given in Fig. 2(c) reveal that the width of the E^1_{2g} peak relative to that of the A_{1g} peak is lower in the synthesized MoS_2 nanosheet than in mechanically exfoliated-MoS_2 (the black dotted line), which can be attributed to planar vibration (E^1_{2g}) being strongly related to the randomly distributed grains found in CVD-grown MoS_2 nanosheets [13]. The FWHM values and peak intensities are also much higher at 750 °C than at 1000 °C, especially when H_2S gas is used for sulfurization.

The quality and crystallinity of the MoS_2 nanosheet were assessed by TEM, with Fig. 3(a,b) showing the nanosheet prior to sulfurization. The use of H_2S (Fig. 3(d,f)) was found to produce an enhanced crystallinity when compared to using sulfur powder at the same annealing temperature (Fig. 3(c,e)). The diffraction patterns and FWHM in the insets of Fig. 3(c–f) show evidence of a six-fold-symmetry following sulfurization [13, 31], with the ring pattern of sample H10 indicating a polycrystalline structure.

The XPS results for the Mo 3*d* and S 2*p* core-levels of samples S7, H7, S10, and H10 are shown in Fig. 4, from which the atomic ratio (stoichiometry) of each sample was obtained based on the ratio of the Mo 3*d* peaks intensity to that of the S 2*p* peak. As shown in Fig. 2, samples prepared in H_2S gas had a comparable atomic concentration to bulk MoS_2, whereas the use of sulfur powder resulted in concentrations either under (750 °C) or over (1000 °C) stoichiometry. This non-stoichiometry is believed to be caused by vacancies and defects generated during synthesis [26, 27, 28]. With either sulfurization agent, the width of the Mo 3*d* and S 2*p* core-level peaks roughly doubled; however, with only sulfur powder, the Mo 3*d* core levels exhibited a peak suggesting oxidization to MoO_3 at a higher binding energy. This phenomenon most likely originates from the substrate, with the oxygen species produced believed to interrupt the crystal structure and degrade the electrical properties of the thin film. This suggests that the use of H_2S gas is the more suitable option for the synthesis of MoS_2 nanosheets.

To further confirm the superiority of H_2S gas over sulfur powder, ultrafast optical-pump-probe measurements of the carrier relaxation time were performed. For this, four different samples of MoS_2 nanosheet were prepared on MgO substrates under conditions of: H_2S at 750 °C (Sample **I**), sulfur powder at 750 °C (Sample **II**), H_2S gas at 1000 °C (Sample **III**), and sulfur powder at 1000 °C (Sample **IV**). A MgO (100) substrate was used as this is not excited by probing measurements with a large band gap of 7.8 eV, as transparent substrates need a band gap larger than the photon energy (3.01 eV) of the pump pulses used for measurement.

Prior to pump-probe measurement, the ground state absorption was measured to determine an appropriate pump-probe wavelength. As can be seen in Fig. 5 (a), the A and B excitons are

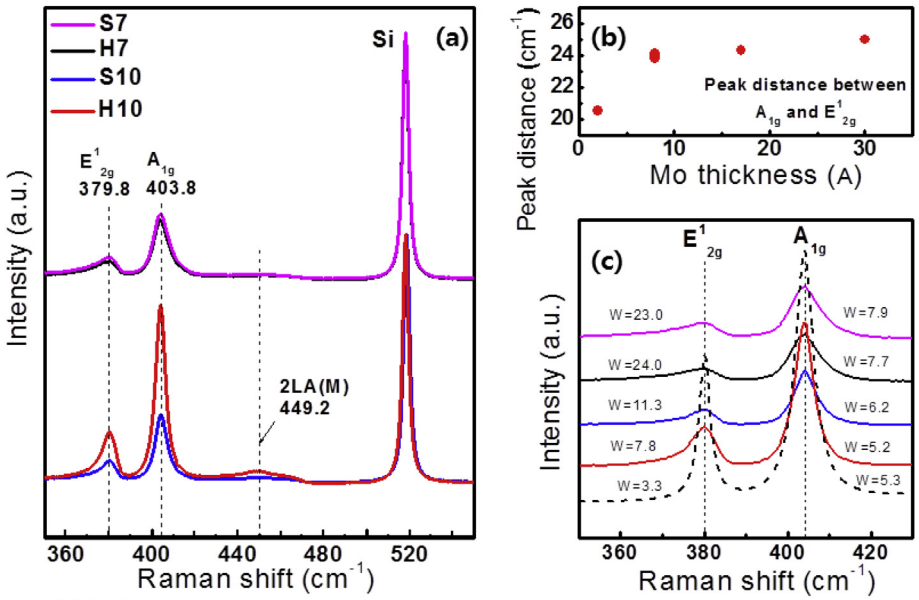

Table 1.

Sample name	temperature	Sulfur source	Sample name	temperature	Sulfur source
S7	750	S powder	H7	750	H_2S gas
S10	1000	S powder	H10	1000	H_2S gas

Fig. 2. Raman spectra of MoS_2 nanosheets produced using H_2S and S at annealing temperatures of 750 and 1000 °C (a),(c). (b) Peak distance of each sputtered Mo film.

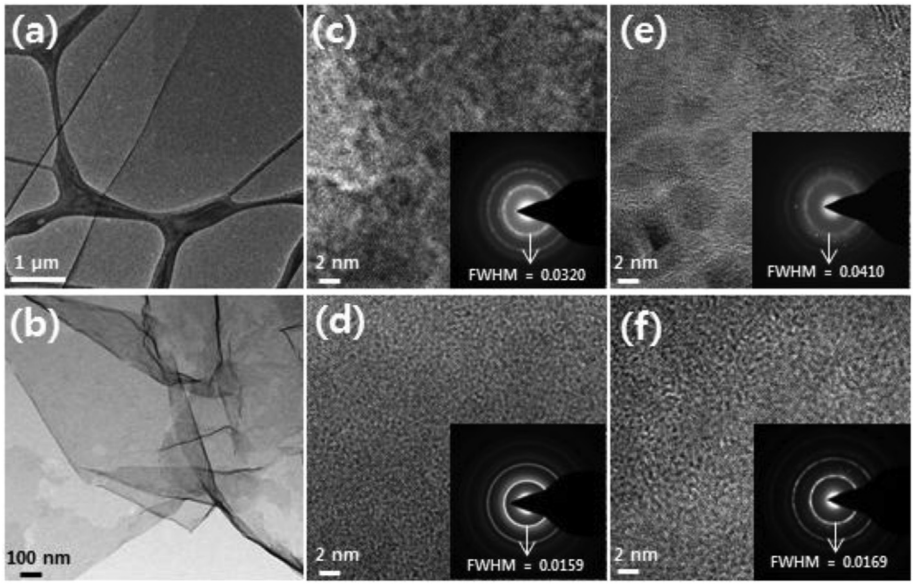

Fig. 3. Low-magnification TEM images of MoS_2 nanosheets (a,b) after transfer, and following sulfurization with (c) H_2S at 750 °C, (d) sulfur powder at 750 °C, (e) H_2S at 1000 °C, and (f) sulfur powder at 1000 °C. Insets show the respective FWHM (nm^{-1}) and diffraction patterns.

associated with direct transitions from a split valence band that results from spin-orbit splitting in the MoS_2 interlayer, with any interaction further modifying this split [32]. All samples exhibit resonance in the 600–700 nm range, which is well known as the direct excitonic transition position of the k point of the Brillouin zone [33]. The transition between peaks A and B [33, 34] is more resolved in samples **I** and **III**, with the appearance of these two peaks suggesting a low level of disorder in the sample [34]. This matches well with the earlier assessment that H_2S gas produces fewer vacancies, and from the ground–state absorption, a probe wavelength of 660 nm used in previous ultrafast pump-probe analyses of MoS_2 thin films [32, 35] was deemed appropriate.

A vacancy is a type of point defect in a crystal, with the scattering of carriers by impurities and lattice defects contributing to their relaxation [36]. Thus, in the pump-probe measurements, the changes in the decay dynamics of the pump-fluence were first observed for the main mechanism of carrier relaxation. All samples were found to show a tendency toward decreasing carrier

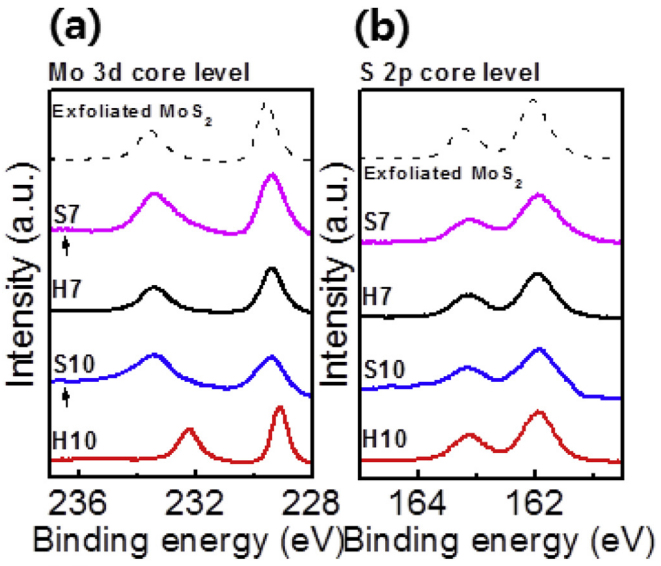

(c)

750°C		1000°C	
S	H_2S	S	H_2S
1:1.3	1:2	1:2.4	1:2.0
Exfoliated MoS_2 = 1: 2.0			

Fig. 4. XPS spectra of MoS_2 nanosheets sulfurized with H_2S or S at 750 or 1000 °C. Peaks for (a) Mo 3*d* and S 2*s*, and (b) S 2p are scaled for clarity. (c) Chemical composition of each MoS_2 nanosheet.

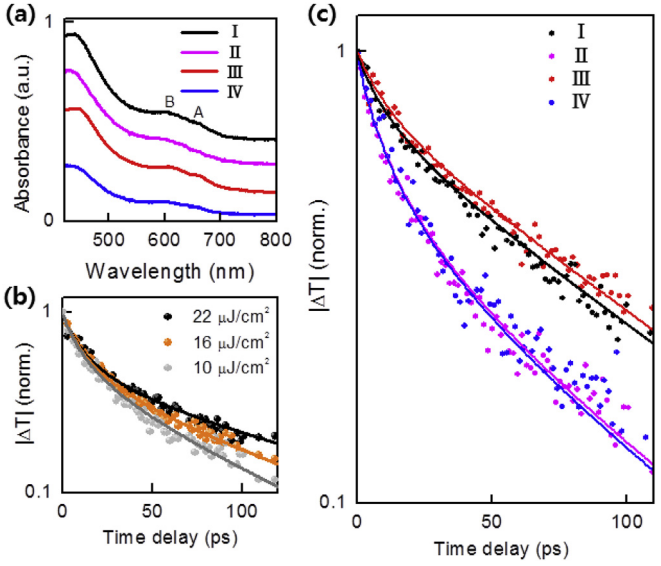

Fig. 5. Ultrafast carrier relaxation dynamics for four different MoS_2 samples. (a) Ground state absorption spectra. (b) Normalized differential transmission signal (dots) of sample **II** using pump and probe beam wavelengths of 400 and 660 nm, respectively. (c) Normalized differential transmission signals (dots) of samples **I**, **II**, **III**, and **IV** with the same pump and probe beam wavelengths as (b). A fixed pump fluence of 16 J/cm^2 was used, and all solid lines are numerical fits obtained using rate equations that describe the vacancy-mediated pump fluence.

relaxation time with increasing pump-fluence; indeed, Sample (Fig. 5(b)) clearly exhibited a slow relaxation behavior with increasing pump-fluence. In a previous report, this slow relaxation was considered to originate from a limited defect state that is rapidly saturated with carriers under the effects of a high fluence [37, 38]. We can therefore assume that the rapid decay and saturation from defects is the major factor in carrier relaxation. In Fig. 5 (c), numerical data for the samples were used to produce rate-equations for a fixed pump-fluence [37] based on:

$$\frac{\mathrm{dn(t)}}{\mathrm{dt}} = -\frac{n(t)}{\tau} + \frac{dT(t)}{dt}$$

$$n(0) = N, T(0) = T$$

where $n(t)$ is the density of mobile charge carriers, γ (= 80 ps) is the carrier life-time, N is the initial density of free charges, $T(t)$ is the density of unoccupied trap states, and T is the initial density of unoccupied trap states. These rate-equations demonstrate that the density of unoccupied trap states reduces over time due to a reduction in the density of mobile charge carriers, with the lifetime of any given defect state $n(t)$ determined by the initial density of unoccupied trap states T. The initial density of free charge N of 2×10^{11} cm^{-2} generated per layer with a pump-fluence of 16 J/cm^2 is obtained by using the method suggested by Shi et al. [32] From the fitted results in Fig. 5(c), it is clear that the relaxation dynamics of a carrier are not influenced by the annealing temperature; however, the carrier life-time is longer when using H_2S instead of sulfur. The initial density of unoccupied trap states in Sample A, B, C, and D was 28, 55, 25, and 56, respectively, indicating that the number of defects is effectively halved by using H_2S. Thus, the change in defects and vacancies is substantially greater than the change in crystallinity due to temperature.

4. Conclusion

This study has demonstrated that the sulfurization can provide effective control over the thickness and area of a MoS_2 nanosheet. The electrical properties of the nanosheet were found to be closely linked to the number of defects and vacancies, which in turn were affected by the sulfurization agent used to a far greater extent than is seen in CVD. This means that a better outcome in terms of ensuring a low sulfur vacancy and high crystallinity can be achieved by using H_2S gas rather than sulfur powder. It is hoped that these results will further the development of 2D-TMDC nanosheets and lead to more advanced sulfurization processes.

Acknowledgements

This research was supported by Basic Science Research Program through the National Research Foundation of Korea (NRF) funded by the Ministry of Education, Science and Technology (No. 2015R1D1A1A01060064), the National Research Foundation of Korea (NRF) grant funded by the Korea government (MSIP) (No. NRF-2014R1A2A1A11052588), the Center for Integrated Smart Sensors funded by the Ministry of Science, ICT & Future Planning as Global Frontier Project (CISS-2011-0031848), Korea Evaluation Institute of Industrial Technology (KEIT) funded by the Ministry of Trade, Industry and Energy (MOTIE) (Project No. 10050296, Large scale (Over 8″) synthesis and evaluation technology of 2D chalcogenides for next generation electronic devices), and the Institute of BioMed-IT, Energy-IT and Smart-IT Technology (BEST), a Brain Korea 21 plus program, Yonsei University.

References

[1] M. Xu, T. Liang, M. Shi, H. Chen, Chem. Rev. 113 (2013) 3766.
[2] S. Kim, A. Konar, W.-S. Hwang, J.H. Lee, J. Lee, J. Yang, C. Jung, H. Kim, J.-B. Yoo, J.-Y. Choi, Y.W. Jin, S.Y. Lee, D. Jena, W. Choi, K. Kim, Nat. Commun. 3 (2012) 1011.

[3] H. Wang, L. Yu, Y.-H. Lee, Y. Shi, A. Hsu, M.L. Chin, L.-J. Li, M. Dubey, J. Kong, T. Palacios, Nano Lett. 12 (2012) 4674.
[4] F.K. Perkins, A.L. Friedman, E. Cobas, P.M. Campbell, G.G. Jernigan, B.T. Jonker, Nano Lett. 13 (2013) 668.
[5] D. Voiry, H. Yamaguchi, J. Li, R. Silva, D.C.B. Alves, T. Fujita, M. Chen, T. Asefa, V.B. Shenoy, G. Eda, M. Chhowalla, Nat. Mater 12 (2013) 850.
[6] J. Kibsgaard, Z. Chen, B.N. Reinecke, T.F. Jaramillo, Nat. Mater 11 (2012) 963.
[7] H.S. Lee, S.-W. Min, Y.-G. Chang, M.K. Park, T. Nam, H. Kim, J.H. Kim, S. Ryu, S. Im, Nano Lett. 12 (2012) 3695.
[8] N. Perea-López, A.L. Elías, A. Berkdemir, A. Castro-Beltran, H.R. Gutiérrez, S. Feng, R. Lv, T. Hayashi, F. López-Urías, S. Ghosh, B. Muchharla, S. Talapatra, H. Terrones, M. Terrones, Adv. Funct. Mater 23 (2013) 5511.
[9] J.S. Ross, S. Wu, H. Yu, N.J. Ghimire, A.M. Jones, G. Aivazian, J. Yan, D.G. Mandrus, D. Xiao, W. Yao, X. Xu, Nat. Commun. 4 (2013) 1474.
[10] Y. Li, C.-Y. Xu, L. Zhen, Appl. Phys. Lett. 102 (2013) 143110.
[11] K. Lee, H.-Y. Kim, M. Lotya, J.N. Coleman, G.-T. Kim, G.S. Duesberg, Adv. Mater 23 (2011) 4178.
[12] Y.-C. Lin, W. Zhang, J.K. Huang, K.K. Liu, Y.H. Lee, C.T. Liang, C.W. Chu, L.J. Li, Nanoscale 4 (2012) 6637.
[13] Y. Zhan, Z. Liu, S. Najmaei, P.M. Ajayan, J. Lou, Small 8 (2012) 966.
[14] H. Hadouda, J. Pouzeta, J.C. Bernedea, A. Barreaub, Mater. Chem. Phys. 42 (1995) 291.
[15] X. Wang, H. Feng, Y. Wu, L. Jiao, J. Am. Chem. Soc. 135 (2013) 5304.
[16] J.-G. Song, J. Park, W. Lee, T. Choi, H. Jung, C.W. Lee, S.-H. Hwang, J.M. Myoung, J.-H. Jung, S.-H. Kim, C. Lansalot-Matras, H. Kim, ACS Nano 7 (2013) 11333.
[17] Y.-H. Lee, L. Yu, H. Wang, W. Fang, X. Ling, Y. Shi, C.-T. Lin, J.-K. Huang, M.-T. Chang, C.-S. Chang, M. Dresselhaus, T. Palacios, L.-J. Li, J. Kong, Nano Lett. 13 (2013) 1852.
[18] S. Balendhran, J.Z. Ou, M. Bhaskaran, S. Sriram, S. Ippolito, Z. Vasic, E. Kats, S. Bhargava, S. Zhuiykov, K. Kalantar-Zadeh, Nanoscale 4 (2012) 461.
[19] S. Najmaei, Z. Liu, W. Zhou, X. Zou, G. Shi, S. Lei, B.I. Yakobson, J.-C. Idrobo, P.M. Ajayan, J. Lou, Nat. Mater. 12 (2013) 754.
[20] A.M. van der Zande, P.Y. Huang, D.A. Chenet, T.C. Berkelbach, Y.M. You, G.-H. Lee, T.F. Heinz, D.R. Reichman, D.A. Muller, J.C. Hone, Nat. Mater 12 (2013) 554.
[21] D.R. Alfonso, Surf. Sci. 602 (2008) 2758.
[22] S. Wang, C. An, J. Yuan, Materials 3 (2010) 401.
[23] J.A. Rodriguez, S. Chaturvedi, M. Kuhn, J. Hrbek, J. Phys. Chem. B 102 (1998) 5511.
[24] X.L. Li, J.P. Ge, Y.D. Li, Chem. Eur. J. 10 (2004) 6163.
[25] Y. Feldman, E. Wasserman, D.J. Srolovitz, R. Tenne, Science 267 (1995) 222.
[26] W. Zhou, X. Zou, S. Najmaei, Z. Liu, Y. Shi, J. Kong, J. Lou, P.M. Ajayan, B.I. Yakobson, J.-C. Idrobo, Nano Lett. 13 (2013) 2615.
[27] S. Tongay, J. Suh, C. Ataca, W. Fan, A. Luce, J.S. Kang, J. Liu, C. Ko, R. Raghunathanan, J. Zhou, F. Ogletree, J. Li, J.C. Grossman, J. Wu, Sci. Rep. 3 (2013) 2657.
[28] S. Helveg, J.V. Lauritsen, E. Laegsgaard, I.I. Stensgaard, J.K. Norskov, B.S. Clausen, H. Topsoe, F. Besenbacher, Phys. Rev. Lett. 84 (2000) 951.
[29] C. Lee, H. Yan, L.E. Brus, T.F. Heinz, J. Hone, S. Ryu, ACS Nano 4 (2010) 2695.
[30] S.-L. Li, et al., ACS Nano 6 (2012) 7381.
[31] Y.-H. Lee, H. Miyazaki, H. Song, H. Kuramochi, S. Nakaharai, K. Tsukagoshi, Adv. Mater 24 (2012) 2320.
[32] H. Shi, R. Yan, S. Bertolazzi, J. Brivio, B. Gao, A. Kis, D. Jena, H.G. Xing, L. Huang, ACS Nano 7 (2013) 1072.
[33] K.F. Mak, C. Lee, J. Hone, J. Shan, T.F. Heinz, Phys. Rev. Lett. 105 (2010) 136805.
[34] G. Eda, H. Yamaguchi, D. Voiry, T. Fujita, M. Chen, M. Chhowalla, Nano Lett. 11 (2011) 5111.
[35] R. Wang, B.A. Ruzicka, N. Kumar, M.Z. Bellus, H.-Y. Chiu, H. Zhao, Phys. Rev. B 86 (2012) 045406.
[36] K. Ishioka, M. Hase, M. Kitajima, K. Ushida, Appl. Phys. Lett. 78 (2001) 3965.
[37] P. Parkinson, H.J. Joyce, Q. Gao, H.H. Tan, X. Zhang, J. Zou, C. Jagadish, L.M. Herz, M.B. Johnston, Nano Lett. 9 (2009) 3349.
[38] K. Lui, F. Hegmann, J. Appl. Phys. 93 (2003) 9012.